FUDMA Journal of Sciences (FJS)
ISSN online: 2616-1370
ISSN print: 2645 - 2944
Vol. 9 No. 5, May, 2025, pp 187 - 195
DOI: https://doi.org/10.33003/fjs-2025-0905-3560

STRUCTURAL, ELECTRONIC AND OPTICAL PROPERTIES OF BORON DOPED MONOLAYER GALLIUM ARSENIDE (GaAs) FOR OPTOELECTRONIC APPLICATION: A DFT STUDY

***[1]Anas Manga, [1,2,3]Yahaya Saadu Itas, [1]Sadiq Abubakar Dalhatu, [1]Aliyu Mohammed Aliyu, [1]Asmau Muhammad Hassan, [4]Mustapha Bello and [1]Abdullahi Abubakar**

[1]Department of Physics, Saadu Zungur University, Gadau -Nigeria
[2]NanoScience and Technology Research Group, Department of Physics, Saadu Zungur University, Bauchi-Nigeria
[3]Applied Physics and Radiation Technologies Group, CCDCU, School of Engineering and Technology, Sunway University, 47500 Bandar Sunway, Selangor, Malaysia
[4]Department of Physics, Federal College of Education (Technical) Omoku, Rivers state

*Corresponding authors' email: anasman@basug.edu.ng; anasmanga002@gmail.com

ABSTRACT

This work carried out investigations on the optoelectronic properties of two-dimensional gallium arsenide under some specific conditions. To achieve the aim and objectives of this research, detailed analysis of electronic, structural and optical absorptions is reported. The first principles calculations method within the density functional theory framework was used to study the structural, electronic and optical properties of boron (B) doped monolayer GaAs. The calculated lattice constants with PBE-GGA are 7.9871 Å, and 6.5861 Å for "a" and "c" respectively. The bandgap value of 0.43 eV was obtained for the undoped monolayer GaAs. When 6.25% of B is introduced into monolayer GaAs, the doping effects modified the band gap from 0.43 to 0.29 eV. Also, by introducing 12.50% of B to monolayer GaAs, the band gap value reduced to 0.12 eV. Our findings confirmed that boron doping narrows the energy band gap of monolayer GaAs semiconductor material. The results of optical absorption indicated that 6.25% B doped monolayer GaAs and 12.50% B monolayer GaAs have strong absorption behavior in the visible light frequency, which depicts its suitability for optoelectronic applications such as solar cells. The study revealed that band gap engineering using boron effectively allowed better control of electronic and optical properties of monolayer (2D) GaAs semiconductor, and enhances visible light absorption, making it superior to undoped GaAs for solar cells.

Keywords: Gallium arsenide, Optoelectronics, Monolayer, Visible light, DFT, Boron doping

INTRODUCTION

Currently, the global community is actively in search of more materials for optoelectronic applications. Because the existing ones are consistently overused, which may lead to some terminal point in terms of abundance. Other reasons for the search of alternative materials for optoelectronics is related to power efficiency and stability (Nowsherwan *et al.,* 2024). Efficient optoelectronic materials must possess large surface area, low electron hole recombination, high thermal stability and versatile mechanical strength (Znidi *et al.,* 2024). Discovery of graphene has attracted a lot of interests in 2D materials especially semiconductors (Tiwari *et al.,* 2020). Several 2D semiconductors such as transition metal dichalcogenides (TMDs), silicon, group III, monochalcogenides and so on were used as good materials for optoelectronics, photocatalysts and spintronics because of their band gap and fast carrier transport system (Saadu *et al.,* 2024). Due to their versatile performance, 2D materials have gain much attention due to their excellent contribution to nanoelectronics, optoelectronic and clean energy conversion (Itas *et al.,* 2023). In the review research by Wang et al, optoelectronic properties of graphene can be improved by changing its shape through combination with other nanomaterials (Wang *et al.,* 2019). The wide band gaps of several nanomaterials have been modified in order to actively promote their optoelectronic behaviors. For example, hexagonal boron nitride (h-BN) has been doped with carbon, which improved it capacity to work as solar cell material (Cui & Xue, 2024).Other researchers have tried to bring heavy materials to optoelectronic environments. This is because they are frequently being ignored despite their versatile optoelectronic characteristics. Youngchan experimentally synthesized a two-dimensional form of molybdenum disulfide (MoS_2) under controlled conditions. It was found the synthesized MoS_2 can actively work as a better candidate for photocatalysis (Kim, 2022).

A semiconductor called gallium arsenide (GaAs) is employed in many technological and scientific applications, including FETs and LEDs, among others (Mishra, 2020). Investigations on its activity in relation to photocatalytic processes are still ongoing. GaAs is widely studied in bulk form, However, with the emergence of two-dimensional (2D) materials, interest has shifted toward exploring the behavior of GaAs at the monolayer level, its monolayer (two-dimensional) properties under boron doping remain insufficiently explored. GaAs monolayer's other characteristics also need to be further investigated. Due to their potential use in photonic, electronic, and optoelectronic devices like thin films solar cells, diode lasers, blue and green light-emitting diodes, metal insulator semiconductor photodetectors, and III-V semiconductors based on GaAs, these materials are currently promising materials in vast scientific and technological usefulness(Yang *et al.,* 2022). Metal-oxide semiconductor capacitor (MOSCAP) and High-Electron Mobility Transistor (HEMT) Electrooptic Waveguide Modulators (Lin & Lu, 2023).

First-principles calculations within the framework of density functional theory (DFT) is the method of choice for investigating material properties at the ground state. DFT in principle provides an exact description of material physical properties at ground states although approximations become necessary. In this work, structural, electronic and optical properties calculations are performed within DFT framework as implemented in Quantum Espresso simulation package (Giannozzi *et al.*, 2017). We made the choice of boron as the model dopant in this research because boron is compatible with the GaAs crystal structure, which

allows efficient incorporation into the lattice without causing significant lattice deformations. It is a group III atom whose valence electrons are three. This makes it effective p-type impurity. Therefore, boron atoms create holes in GaAs lattice which promotes its conductivity. Boron-doped GaAs exhibits good thermal stability, which is important for maintaining performance in devices that operate at high temperatures (Khanna, 2017).

MATERIALS AND METHODS

Computational Methods

In this research, the first principles calculations of the structural, electronic and optical properties of the system under study were carried out within the DFT implemented in quantum ESPRESSO codes. In this work, the geometric structure of the pristine GaAs (2D) monolayer was generated from materials project data base (Rouzhahong *et al.,* 2020). Thereafter, the 2×2 super cell of monolayer GaAs monolayer was constructed using BURAI software. The first-principles DFT calculation were carried out using pseudopotential method with plane-wave as a basis set and norm-conserving pseudopotentials generated within the PBE-GGA (Perdew-Burke-Ernzerhof Generalized Gradient Approximation) framework were used to describe the electron-ion interactions. Doping was performed by replacing Ga atoms of with B atoms in concentrations of 6.25% and 12.50% respectively. To achieve balance between computational cost and accuracy, various convergence test were performed on the basis of kinetic energy cut-of values and k-sampling of the Brillouin zone (Mustapha *et al.,* 2022),(Adamu *et al.,* 2020). Calculations of the electronic and optical properties of the pristine and B-doped GaAs monolayer was performed using the generalized gradient (GGA) approximation method in terms of Perdiew-Burke-Emzerhop (PBE) exchange correlation functional as implemented in quantum ESPRESSO codes (Giannozzi *et al.,* 2009),(Alhassan & Albaba, 2024). The PBE-GGA functional was employed due to its computational efficiency and its established reliability for predicting structural and electronic properties of semiconductors. While hybrid functional such as HSE06 offer improved accuracy for bandgap calculations, their significantly higher computational cost limits their practically for large supercells and extensive doping studies like those conducted here. Analysis of the structural, electronic and optical properties of the considered B-doped GaAs monolayer were examined based on the materials' response to visible light in the electromagnetic spectrum

RESULTS AND DISCUSSION

Convergence Test of E_Cut and k_Points

Within the DFT framework, a fundamental need for first-principle calculations is to compute the convergence test before calculating the structural, electronic, and optical characteristics. The resulting convergence tests with regard to the plane wave kinetics energy cut-off and k-points mesh are shown in Figure 1. As can be seen from the convergence test in Figure 1(a), the total energy changes significantly from the kinetic energy cut-off of 05 Ry to 50 Ry and then almost stays nearly constant at 60 Ry. Consequently, we choose 70 Ry as the kinetic energy cut-off number in all of our computations. Figure 1(b) shows the fluctuations of the total energy with k-points. However, the overall energy varies significantly with the number of k-points, indicating a value that has well-converged at precise locations. On the other hand, the total energy rises from 1 x 3 x 3 to 1 x 6 x 6 k-point grids and then nearly stays constant at 1 x 8 x 8 k-point. Consequently, we utilized the 1×9×9 k-point in all of our computations

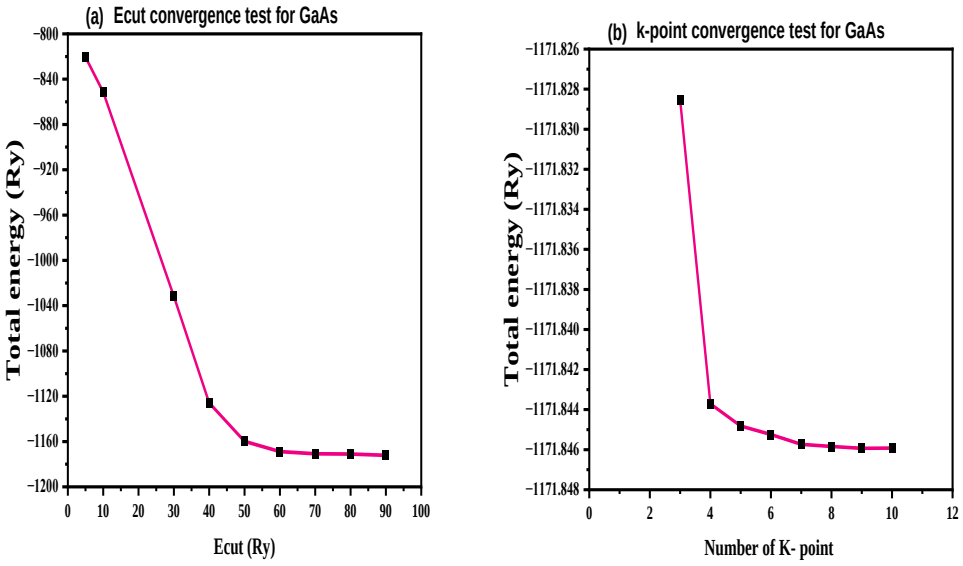

Figure 1: (a) The convergence of total energy with respect to the kinetic energy cut-Off. (b) The convergence of the total energy with respect to the k-points grids

Structural Properties of Pure and Doped Monolayer GaAs

The structure relaxation via Quantum ESPRESSO code employing various exchange potentials was carried out by reducing the total energy with regard to the unit cell in order to determine the equilibrium structural ground state parameters of the Monolayer GaAs molecule, such as the lattice constants. The structural optimization procedure started with the monolayer GaAs compound's experimental lattice parameters. Figure 2(a) displays the geometric structures for monolayer GaAs, Figure 2(b) and Figure 2 (c) display the geometric structures for 6.25% B doped monolayer GaAs and 12.50% B doped monolayer GaAs respectively. With a vacuum in the Z direction, the GaAs

monolayer was positioned at the X-Y plane. One-unit cell of the GaAs monolayer has one Ga atom and one As atom, as seen in Fig. 2. The GaAs monolayer structure is a member of the monolayer honeycomb structure, which is created by repeating six membered rings (Rouzhahong *et al.*, 2020). The As atom coordinates itself thrice with three Ga atoms, and each Ga atom coordinates three times with three As atoms. The computed lattice parameter in monolayer are a= 7.9871, and c= 6.5861. the computed lattice parameter for monolayer GaAs in the wurtzite phase exhibits a modification in the in-plane lattice constant, with an increasing from approximately 3.98 Å to 7.98 Å. This variation is attributed to the of a 2×2 supercell expansion, a standard technique in computational materials science for simulating monolayer systems (Cahangirov & Ciraci, 2009),(De & Pryor, 2010). While the c parameter remains consistent at 6.58 Å, reflecting the vertical spacing of the GaAs structure, the expansion of 'a' is a direct result of the increased unit cell in the in-plane direction to accommodate the monolayer and introduce necessary vacuum space, in accordance with common computational practices (Glas *et al.*, 2013),(Surnev *et al.*, 2024). This outcome is consistent with previous studies employing similar supercell techniques to model the structural properties of low-dimensional materials, such as monolayer and thin films. Specifically, earlier works on 2D GaAs and related systems have demonstrated that supercell expansion results in modifications to the lateral lattice constants without significantly affecting the vertical spacing (Dridi *et al.*, 2003),(Rasmussen & Thygesen, 2015). The GaAs monolayer buckling height (h) is 0.41 Å, and the Ga-As bond length (2.41 Å), this has similar value to a prior researcher's (Mishra, 2020), (Rouzhahong *et al.*, 2020)

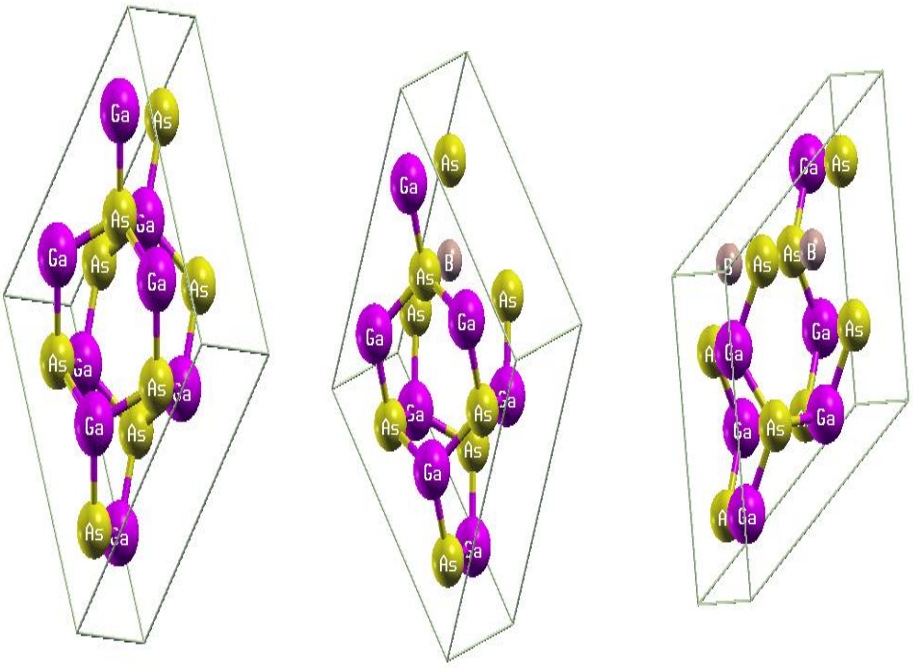

Figure 2: Schematic diagram of Geometric Crystal of (a) Pure Monolayer GaAs (b) 6.25% B doped Monolayer GaAs (c) 12.50% B doped Monolayer GaAs

Electronic Properties of Pure and Doped Monolayer GaAs

The electronic structure and band gap energy of semiconductors have a significant impact on how well they function under visible light (Itas, Suleiman, Ndikilar, Lawal, Razali, & Danmadami, 2023), (Mustapha et al., 2022), (Itas, Isah, et al., 2023). The bandgap of semiconductor material should be smaller than 3 eV for best results in order to expand photo absorption into the visible region and make efficient use of solar energy (Itas, Isah, et al., 2023). Both un-doped and doped monolayer GaAs predicted electronic band structure is displayed along the first Brillouin zone's high symmetry point, Γ-M-K-Γ-A-L-H-A-L-M-K-H as shown in Figure 3. The energy of band structure separation is plotted from $-5.0\ eV$ to $5.0\ eV$ in the case of undoped and doped monolayer GaAs. In this work, we first analyzed the electronic band structure of the pristine monolayer GaAs semiconductor, and the results are shown in Figure. 3(a) The results showed a band gap of 0.43 eV, indicating the energy difference between its valence band (VB) and conduction band (CB) agrees with the obtained 0.42 eV, experimental results(Ma et al., 2020) . in this work, a bandgap of 0.43 eV was obtained for monolayer GaAs using DFT with the PBE-GGA functional. This result aligns with trends observed in earlier studies that used similar computational methods. For instance, (Anua *et al.*, 2012), reported a PBE-GGA bandgap of 0.329 eV, while (Madu & Onwuagba, 2010)obtained a value of approximately 0.35 eV using FPLAPW method within the same functional. Thought slightly lower than the present value, these results reflect the known underestimation of bandgap by PBE-GGA. The small variation in reported values can be attributed to differences in computational parameters, structural models, and dimensionality. The present result is consistent with existing literature and supports the reliability of PBE-GGA in capturing the electronic properties of monolayer GaAs. The valence band represents the highest energy level filled with electrons at absolute zero temperature, while the conduction band is the energy level above the valence band where electrons can move freely. This means that at room temperature, only electrons with energies higher than 0.43 eV can overcome the bandgap and transition from the valence band to the conduction band, enabling electrical conductivity. Therefore, monolayer GaAs in its current state is suitable for use as a photocatalyst, since the obtained band gap is much higher than 0 eV. In its intrinsic state, monolayer GaAs has equal numbers of electrons and holes. The Fermi energy level (E_F)

lies near the middle of the bandgap. When monolayer GaAs is doped with boron (B) atoms, interesting changes occur in its electronic properties. Doping introduces impurity levels within the bandgap, altering the semiconductor's conductivity characteristics (Pramanik et al., 2024),(Itas, Suleiman, Ndikilar, Lawal, Razali, Ullah, et al., 2023). Boron, being a group III element, introduces acceptor levels in GaAs, creating holes in the valence band. When 6.25% Boron atom is introduced into the lattice structure of monolayer GaAs, it replaces a Gallium atom. Since boron has one fewer valence electron than Gallium, it creates a hole (missing electron) in the valence band. This increases the concentration of holes and makes the material a P-type semiconductor. The introduction of this hole acceptor state moves the Fermi energy level (E_F) closer to the valence band. As shown in Figure 3(b) Doping monolayer GaAs with one boron atom reduces the bandgap to 0.29 eV which is less than 3 eV, and hence can be a better photocatalyst, which also agrees with the experimental range for photocatalysts. This reduction indicates that the energy required for electrons to transition from the valence band to the conduction band decreases (Wu *et al.,* 2021). Consequently, the material becomes more conductive as the number of available charge carriers (holes) increases due to boron doping (Cao *et al.,* 2022). As shown in Figure. 3(c) a 12.50% boron atom creates another hole. This further increases the concentration of holes and pushes the Fermi level even closer to the valence band. The bandgap is reduced even further to 0.12 eV due to the presence of two holes' acceptor states. Doping monolayer GaAs with boron atoms alters its electronic properties by reducing the bandgap, enhancing its conductivity, and shifting the Fermi energy. These changes are crucial for tailoring the material's electrical behavior and making it suitable for various semiconductor device applications (Itas *et al.,* 2024), (Balcı *et al.,* 2017).

To gain a comprehensive understanding of the nature of the energy gap, the total density of state (DOS) and partial density of state (PDOS) were analyzed. The DOS and partial density of states (PDOS) results are shown in Figures 4 and 5, respectively, in all three cases (a, b, and c), the DOS plots exhibit lower peaks at higher energies, corresponding to the conduction band. Conversely, higher peaks at lower energies represent the valence band. The position of the Fermi level (E = 0 eV) is evident in both Figures. The pristine monolayer GaAs (Figure 4a) shows a valence band ranging from -15.80 eV to 0 eV and a conduction band between 0.0 eV and 4.20 eV. The peak of the valence band is located at -15.34 eV. Introducing boron dopants (Figures 4b and 4c) demonstrate some noticeable effect; The valence band remains relatively unchanged, spanning -15.75 eV to 0 eV in both cases. The conduction band shows a slight upward shift in energy distribution. In Figure 4b (6.25% dopant), the conduction band ranges from 0.0 eV to 4.39 eV, with a peak at -15.22 eV. This effect becomes more pronounced with 12.5% B dopants (Figure 4c), where the conduction band spans 0.0 eV to 5.21 eV and the peak reaches -15.18 eV. In an intrinsic semiconductor (undoped), the Fermi level lies near the middle of the bandgap. Doping disrupts this equilibrium, causing the Fermi level to shift closer to the valence band in p-type doping. This shift, in turn, influences the distribution of electrons in the energy bands (Raship *et al.,* 2023). The upward movement of the conduction band reflects the introduction of additional energy states due to the presence of holes (Samaki *et al.,* 2023). The PDOS plot in Figure 5 shows how each type of atom (and its orbitals) contributes to the overall distribution of electrons in the 6.25% B-doped GaAs. The combined contribution of these orbitals shapes the overall electronic structure of the 6.25% B-doped GaAs material. The valence band is primarily formed by the overlap of Ga 2p and As 2p orbitals. The conduction band likely involves contributions from Ga 4f, As 4d, and possibly Ga 3d and As 3d orbitals at higher energies. The presence of the B 2p peak near the valence band confirms the p-type doping and signifies the introduction of acceptor states by Boron

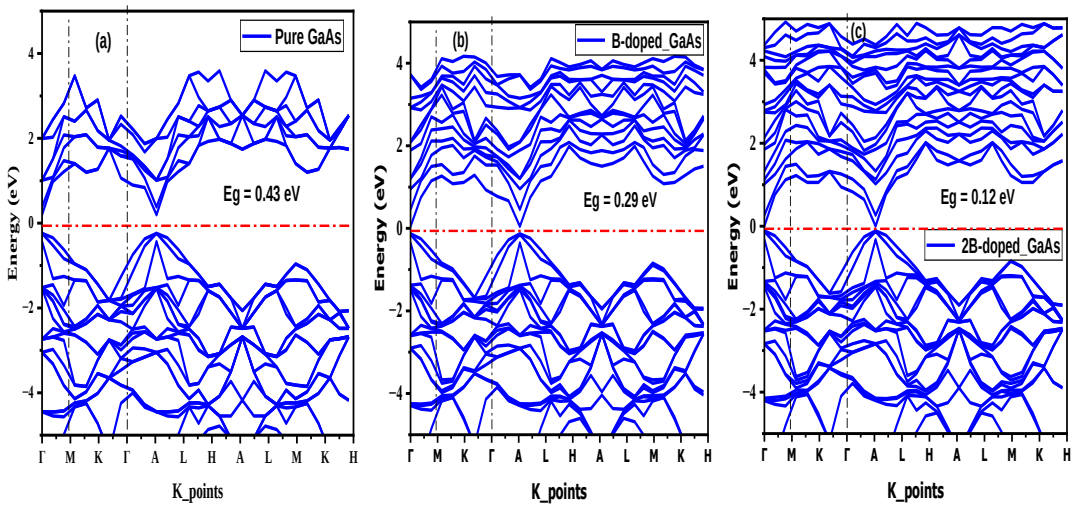

Figure 3: Electronic band structures of (a) pristine Monolayer GaAs (b) 6.25% B-doped Monolayer GaAs and (c) 12.5% B-doped Monolayer GaAs

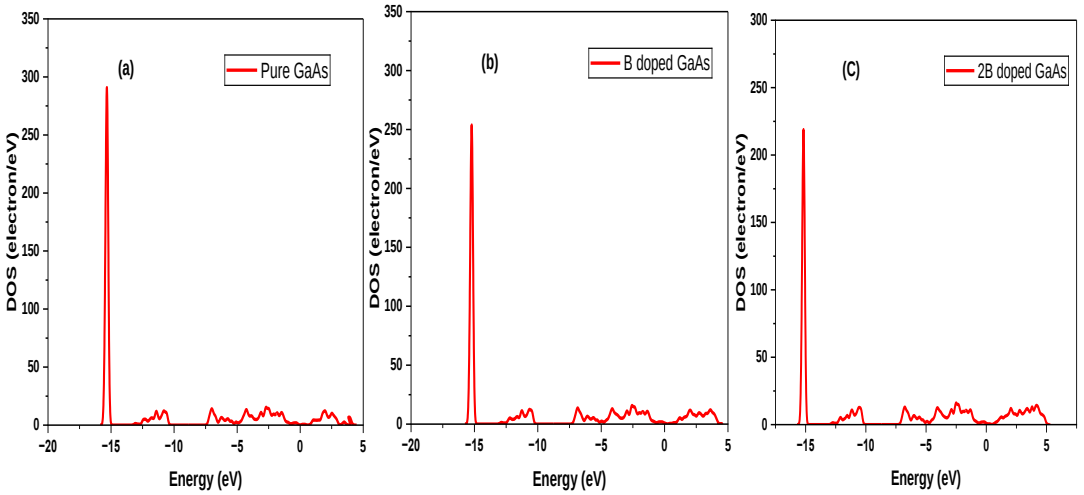

Figure 4: Electronic density of states of (a) pristine Monolayer GaAs (b) 6.25% B-doped Monolayer GaAs and (c) 12.50 B-doped Monolayer GaAs

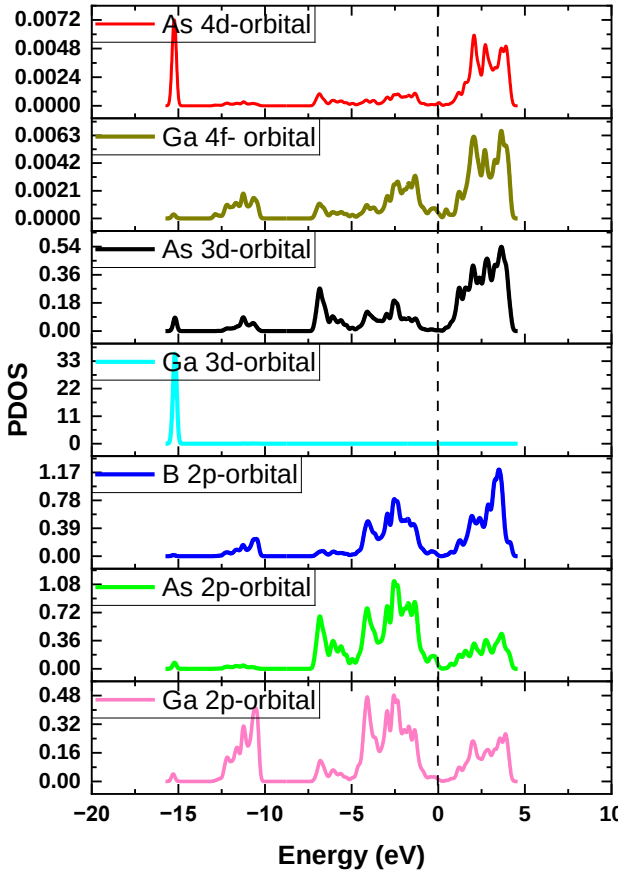

Figure 5: Partial density of states (PDOS) of 6.25% B-doped Monolayer GaAs

Optical Properties of Pure and Doped Monolayer GaAs

To determine a material's utility and suitability for an optoelectronic application, one must comprehend its optical behavior ("Lead-Free Perovskites for Flexible Optoelectronics," 2024),(Zou et al., 2024). This is because electronic structure has a substantial correlation with optical phenomena (Ishikawa *et al.*, 2019). in the current study, geometry and electronic structure of monolayer GaAs with the element being swapped has been adjusted. This can be seen in the electronic band structure analysis. This is found to be in good agreement with experimental investigations which reported that that the dopant element concentration affects the optical characteristics of doped materials(Itas, *et al.*, 2023).

In order to describe the said parameter quantitatively, it is essential to evaluate dielectric function. Dielectric function is the ratio of the permittivity of a material to the permittivity of free space, whereas permittivity is the measure of the resistance of a material when an electric field is induced in a material (Scarpa *et al.*, 2024). The dielectric function consists of real ($\varepsilon_1(\omega)$) and imaginary part ($\varepsilon_2(\omega)$). It is represented as follows:

$$\varepsilon(\omega) = \varepsilon_1(\omega) + i\varepsilon_2(\omega) \quad (1)$$

where $\varepsilon_1(\omega)$ is real part and $\varepsilon_2(\omega)$ is imaginary part of the dielectric function. Physical properties and band structure rely strongly on $\varepsilon(\omega)$.

From the knowledge of electronic band structure of a solid, the imaginary part of the dielectric function, $\varepsilon_2(\omega)$ can be calculated from Kubo–Greenwood equation as shown in Equation 4.2:

$$\varepsilon_2(\omega) = \frac{2\pi e^2}{\Omega\varepsilon_0}|\langle\psi_k^c|\hat{u}\times\vec{r}|\psi_k^v\rangle|\delta\left(E_k^c-(E_k^v+E)\right) \quad (2)$$

The calculated imaginary (ε_2) parts of the dielectric functions as a function of the photon energy for undoped and doped monolayer GaAs are shown in Figure 6. To further elucidate the optical characteristics of the three varieties of Monolayer GaAs, Figures 7 and 6 display the spectra depicting the real and imaginary components of the dielectric functions. The peaks in the imaginary segments of the dielectric constants for both undoped and doped monolayer GaAs trace the optical band gaps. As presented in Figure 7 (a), sharp maxima peaks for real dielectric functions were seen. For pure monolayer GaAs, the peak appeared at 45.6 corresponding to 0.35 eV. In terms of 6.25% B doped monolayer GaAs, higher minimum peak was recorded which appeared at very low energy region of 0.3 eV which enhanced optical conductivity while maximum peak recorded appeared at an energy region of 3.03eV. Lower peak was also observed for 12.50% B doped monolayer GaAs but the peaks are at range of visible to ultraviolet, as shown in Figure 7 (c). Based on this both 6.25% B doped monolayer GaAs and 12.50% B doped monolayer GaAs can be regarded as best candidate for optoelectronics applications.

The static dielectric constant for monolayer GaAs is 55.8, the dielectric absorption peak appears near 3.3 eV. Other dielectric constants appear at 132, and 107 for 6.25% B doped monolayer GaAs and 12.50% B doped monolayer GaAs respectively. In all cases the increase in the dielectric peaks were observed between 0 to 3.0 eV as presented in Figure 6(b) and 6(c). In this range, the dielectric constant increases with decrease in the energy gap. The presence of peaks of monolayer GaAs in the imaginary part of the dielectric function indicate the occurrence of inter-band transitions. EELS enables us to obtain the band gap energy from the onset energy of a spectrum that reflects inter-band transitions.

The energy loosed/released by an electron in traversing from one band to another is calculated for both monolayer GaAs, 6.25% B doped monolayer GaAs and 12.5% B doped monolayer GaAs systems. The calculated charge distributions of each of the three materials were presented in Figure 8. In all cases, the peaks of (ω) appear as a result of combined excitations of different photons with various frequencies. The expanded distance of the electron energy loss by the excitons in monolayer GaAs (Fig. 8a) relates to the absorption peak. This shows that the distribution of the valence electrons has fast convergence. More energies are loosed in the x direction than in the y direction for monolayer GaAs, this can be seen by the appearance of peaks at 16.97 eV. Therefore, maximum energy is loosed as a result of the effect of incident electromagnetic radiation with matter. In the 6.25% B doped monolayer GaAs structure and 12.5% B monolayer GaAs, there were maximum energy loss in the y direction than in the x direction, this can be seen from the peak at 13.33 eV and 13.93 presented in Figure. 8(b) and 8(c) respectively. The energy loss region of the EELS in Fig. 8 (a, b and c) is generally less than 50 eV, this is specifically called the valence electron energy loss spectroscopy (VEELS) because it is dominated by the collective excitations of the Plasmon (valence electrons) and inter-band transitions

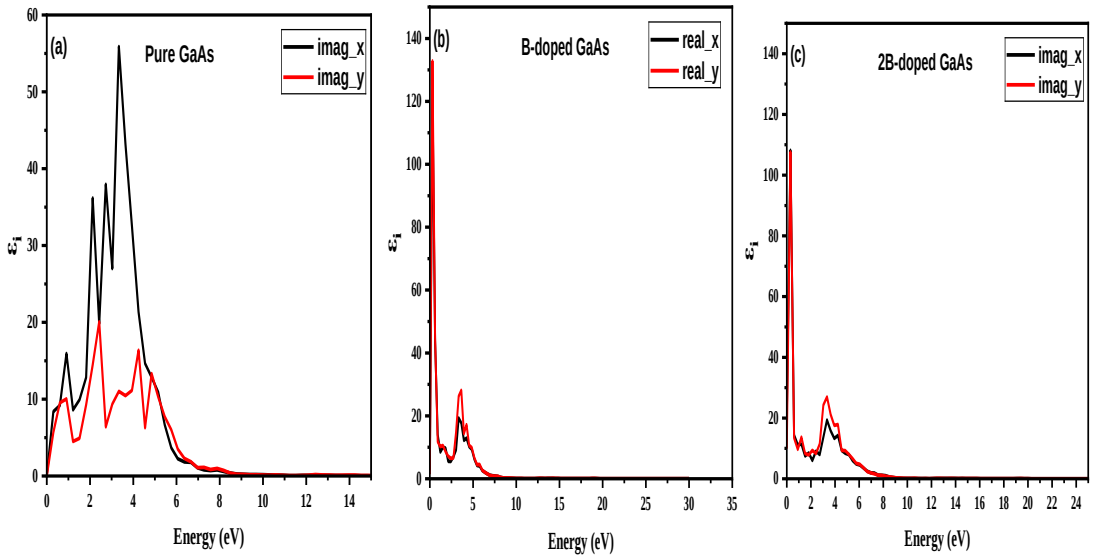

Figure 6: Imaginary dielectric for (a) pristine Monolayer GaAs (b) 6.25% B-doped Monolayer GaAs and (c) 12.50% B-doped Monolayer GaAs

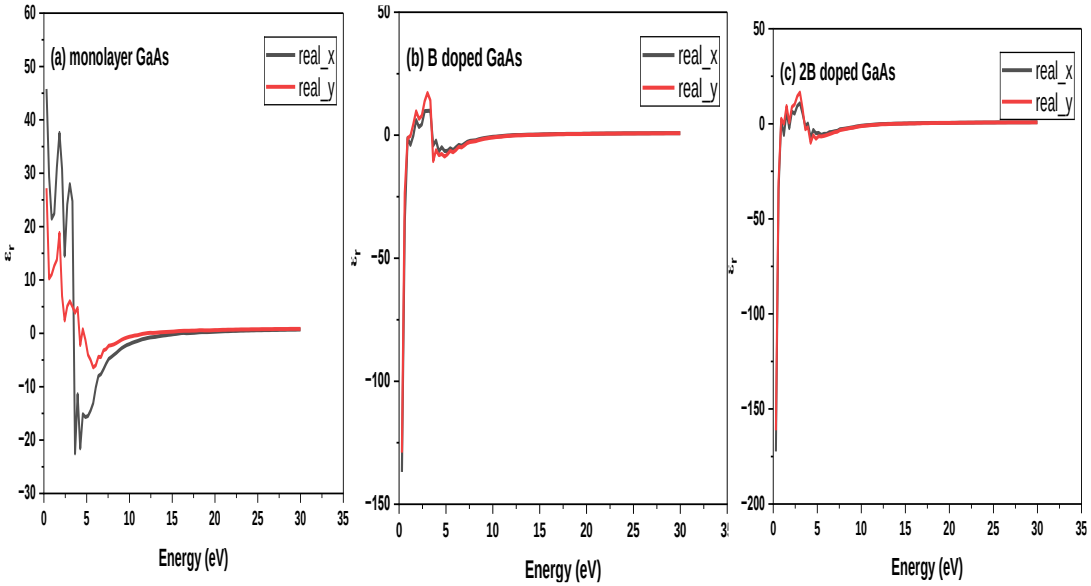

Figure 7: Real dielectric for (a) pristine Monolayer GaAs (b) 6.25% B-doped Monolayer GaAs and (c) 12.50% B-doped Monolayer GaAs

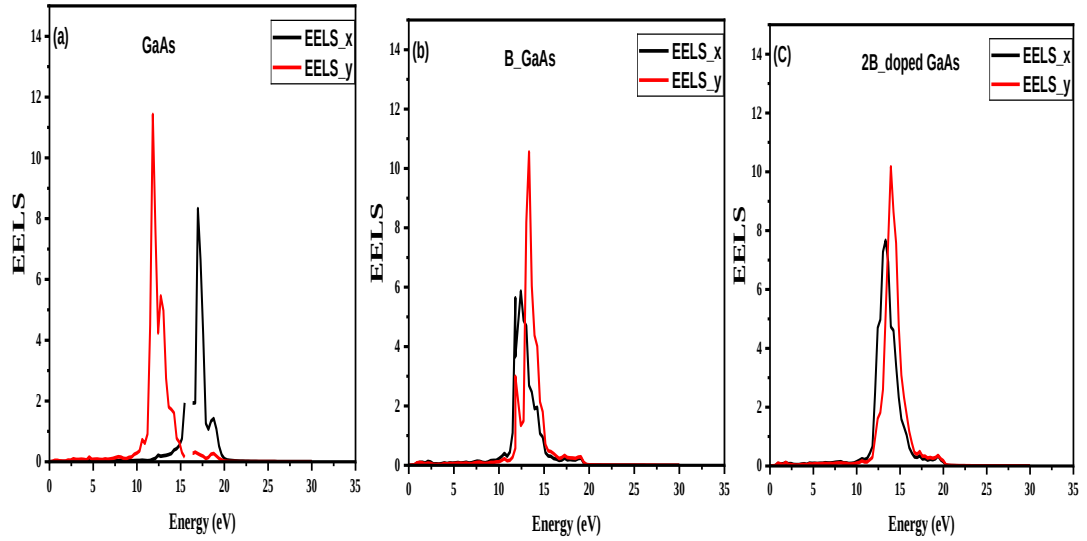

Figure 8: Electron energy loss variations of (a) pristine Monolayer GaAs (b) 6.25% B-doped Monolayer GaAs and (c) 12.50% B-doped Monolayer GaAs

CONCLUSION

To conclude our findings in this paper, we performed investigations on the structural, electronic and optical properties of Boron doped monolayer GaAs based on density functional theory. The results confirmed that undoped monolayer GaAs was found to have a bandgap value of 0.43 eV. The band gap changed from 0.43 to 0.29 eV due to doping effects when 6.25% B atom was added to monolayer GaAs. Additionally, the band gap value decreased to 0.12 eV when 12.5% B atoms were added to monolayer GaAs. Our results verified that boron doping reduces the monolayer GaAs semiconductor material's energy band gap and shift the Fermi energy level closer to the valence band. The results of optical absorptions indicated that B doped monolayer GaAs has strong absorption behavior in the visible light frequency, which depicts its suitability for optoelectronic applications such as telecommunication laser, blue laser, optical fiber, LED traffic lights, photo diodes and solar cells. Dopants' significance in altering the electronic structure of GaAs is revealed by density of states analysis, and the quantitative description of optical properties needed for optoelectronic applications is provided by dielectric function evaluation. All things considered, this study shows that 6.25% and 12.50% of B-doped monolayer GaAs are viable options for light absorption applications, backed by thorough data and explained energy loss fluctuations using electron energy loss spectroscopy

ETHICS STATEMENT

Procedure for data collection and study protocols were permitted by the Bauchi State University Centre for Excellence Research and Innovation and was conducted according to the guidelines declared. Also, no human parts were used in the conduct of this research.

DATA AVAILABILITY STATEMENT

All data that we used in this manuscript regarding quasi-particle energies, bands structure, DOS and optical spectra analysis were analyzed and obtained with the quantum ESPRESSO codes which are freely available at www.quantumespresso.org. Correction to quasi-particle interactions was done via Yambo interacting codes at

www.yambo.org. We have optimized the geometric system of gallium arsenide nanotube by using 'tubegen' database which is freely available at https://turin.nss.udel.edu/research/tubegenonline.html

REFERENCES

Adamu, M. A., Lawal, K., & Saminu, A. (2020). DFT Computation of the Band Structure and Density of State for ZnO Halite Structure using FHI-aims CODE. *FUDMA Journal of Sciences*, *4*(2), Article 2. https://doi.org/10.33003/fjs-2020-0402-231

Alhassan, S. S., & Albaba, A. L. (2024). Structural, Electronic and Magnetic Properties of Vanadium Doped Delafossite CUGAO2: An Ab Initio Study. *FUDMA Journal of Sciences*, *8*(1), Article 1. https://doi.org/10.33003/fjs-2024-0801-2196

Anua, N. N., Ahmed, R., Saeed, M. A., Shaari, A., & Haq, B. U. (2012). DFT investigations of structural and electronic properties of gallium arsenide (GaAs). *AIP Conference Proceedings*, *1482*(1), 64–68. https://doi.org/10.1063/1.4757439

Balcı, E., Akkuş, Ü. Ö., & Berber, S. (2017). Band gap modification in doped MXene: Sc2CF2. *Journal of Materials Chemistry C*, *5*(24), 5956–5961. https://doi.org/10.1039/C7TC01765K

Cahangirov, S., & Ciraci, S. (2009). First-principles study of GaAs nanowires. *Physical Review B*, *79*(16), 165118. https://doi.org/10.1103/PhysRevB.79.165118

Cao, L. C. T., Hakim, L., Hsu, S.-H., Cao, L. C. T., Hakim, L., & Hsu, S.-H. (2022). Boron Doping in Next-Generation Materials for Semiconductor Device. In *Characteristics and Applications of Boron*. IntechOpen. https://doi.org/10.5772/intechopen.106450

Cui, P., & Xue, Y. (2024). Enhancing photovoltaic performance of boron nitride quantum dots: A density functional theory study on carbon doping and amino functionalization. *FlatChem*, *44*, 100625. https://doi.org/10.1016/j.flatc.2024.100625

De, A., & Pryor, C. E. (2010). Predicted band structures of III-V semiconductors in the wurtzite phase. *Physical Review B*, *81*(15), 155210. https://doi.org/10.1103/PhysRevB.81.155210

Dridi, Z., Bouhafs, B., & Ruterana, P. (2003). First-principles investigation of lattice constants and bowing parameters in wurtzite AlxGa1−xN, InxGa1−xN and InxAl1−xN alloys. *Semiconductor Science and Technology*, *18*(9), 850. https://doi.org/10.1088/0268-1242/18/9/307

Giannozzi, P., Andreussi, O., Brumme, T., Bunau, O., Buongiorno Nardelli, M., Calandra, M., Car, R., Cavazzoni, C., Ceresoli, D., Cococcioni, M., Colonna, N., Carnimeo, I., Dal Corso, A., de Gironcoli, S., Delugas, P., DiStasio, R. A., Ferretti, A., Floris, A., Fratesi, G., … Baroni, S. (2017). Advanced capabilities for materials modelling with Quantum ESPRESSO. *Journal of Physics. Condensed Matter: An Institute of Physics Journal*, *29*(46), 465901. https://doi.org/10.1088/1361-648X/aa8f79

Giannozzi, P., Baroni, S., Bonini, N., Calandra, M., Car, R., Cavazzoni, C., Ceresoli, D., Chiarotti, G. L., Cococcioni, M., Dabo, I., Dal Corso, A., de Gironcoli, S., Fabris, S., Fratesi, G., Gebauer, R., Gerstmann, U., Gougoussis, C., Kokalj, A., Lazzeri, M., … Wentzcovitch, R. M. (2009). QUANTUM ESPRESSO: A modular and open-source software project for quantum simulations of materials. *Journal of Physics. Condensed Matter: An Institute of Physics Journal*, *21*(39), 395502. https://doi.org/10.1088/0953-8984/21/39/395502

Glas, F., Ramdani, M. R., Patriarche, G., & Harmand, J.-C. (2013). Predictive modeling of self-catalyzed III-V nanowire growth. *Physical Review B*, *88*(19), 195304. https://doi.org/10.1103/PhysRevB.88.195304

Ishikawa, T., Urasawa, Y., Shindo, T., Okimoto, Y., Koshihara, S., Tanaka, S., Onda, K., Hiramatsu, T., Nakano, Y., Tanaka, K., & Yamochi, H. (2019). Optical Study of Electronic Structure and Photoinduced Dynamics in the Organic Alloy System [(EDO-TTF)0.89(MeEDO-TTF)0.11]2PF6. *Applied Sciences*, *9*(6), Article 6. https://doi.org/10.3390/app9061174

Itas, Y. S., Alotaibi, N. H., Mohammad, S., Haldhar, R., Kim, S.-C., & Hossain, M. K. (2024). DFT studies on structural, electronic and optical properties of aluminum nitride nanotube doped by different concentrations of boron. *Materials Chemistry and Physics*, *320*, 129429. https://doi.org/10.1016/j.matchemphys.2024.129429

Itas, Y. S., Isah, K. A., Nuhu, A. H., Razali, R., Tata, S., A, N. K., Idris, A. M., Ullah, M. H., & Khandaker, M. U. (2023). The potentials of boron-doped (nitrogen deficient) and nitrogen-doped (boron deficient) BNNT photocatalysts for decontamination of pollutants from water bodies. *RSC Advances*, *13*(34), 23659–23668. https://doi.org/10.1039/D3RA03838F

Itas, Y. S., Razali, R., Tata, S., Idris, A. M., & Khandaker, M. U. (2023). Studies of the hydrogen energy storage potentials of Fe- and Al-doped silicon carbide nanotubes (SiCNTs) by optical adsorption spectra analysis. *Journal of Energy Storage*, *72*, 108534. https://doi.org/10.1016/j.est.2023.108534

Itas, Y. S., Suleiman, A. B., Ndikilar, C. E., Lawal, A., Razali, R., & Danmadami, A. M. (2023). Effects of Ir and B co-doping on H2 adsorption properties of armchair carbon nanotubes using Optical Spectra Analysis for energy storage. *Gadau Journal of Pure and Allied Sciences*, *2*(1), Article 1. https://doi.org/10.54117/gjpas.v2i1.58

Itas, Y. S., Suleiman, A. B., Ndikilar, C. E., Lawal, A., Razali, R., Ullah, M. H., Osman, H., & Khandaker, M. U. (2023). DFT Studies of the Photocatalytic Properties of MoS2-Doped Boron Nitride Nanotubes for Hydrogen Production. *ACS Omega*, *8*(41), 38632–38640. https://doi.org/10.1021/acsomega.3c05907

Khanna, V. K. (2017). The temperature-sustaining capability of gallium arsenide electronics. In *Extreme-Temperature and Harsh-Environment Electronics: Physics, technology and applications*. IOP Publishing. https://doi.org/10.1088/978-0-7503-1155-7ch7

Kim, Y. (2022). Controllable synthesis and optoelectronic applications of wafer-scale MoS2 films. *Materials Research Express*, *9*(12), 125004. https://doi.org/10.1088/2053-1591/aca7b3

Lead-free perovskites for flexible optoelectronics. (2024). *Materials Today Electronics*, *8*, 100095. https://doi.org/10.1016/j.mtelec.2024.100095

Lin, Y.-S., & Lu, C.-C. (2023). AlGaN/GaN Metal Oxide Semiconductor High-Electron Mobility Transistors with Annealed TiO2 as Passivation and Dielectric Layers. *Micromachines*, *14*(6), Article 6. https://doi.org/10.3390/mi14061183

Ma, D., Cao, Y., Zhang, J., Deng, Y., Wang, W., & Li, E. (2020). Density functional theory study on the properties of Cu-doped GaAs. *Vacuum*, *175*, 109252. https://doi.org/10.1016/j.vacuum.2020.109252

Madu, C. A., & Onwuagba, B. N. (2010). Energy Band Structure Studies Of Zinc-Blende GaAs and InAs. *Journal of the Nigerian Association of Mathematical Physics*, *16*, 51–56.

Mishra, H. (2020). Exciton-driven giant nonlinear overtone signals from buckled hexagonal monolayer GaAs. *Physical Review B*, *101*(15). https://doi.org/10.1103/PhysRevB.101.155132

Mustapha, B., Lawal, A., Aliyu, A. M., & Dalhatu, S. A. (2022). Density Functional Theory studies of structural, electronic and optical properties of Fluorine Doped Magnesium Hydride: DFT Studies of Structural, Electronic and Optical Properties of F-Doped MgH2. *Gadau Journal of Pure and Allied Sciences*, *1*(2), Article 2. https://doi.org/10.54117/gjpas.v1i2.35

Nowsherwan, G. A., Ali, Q., Ali, U. F., Ahmad, M., Khan, M., & Hussain, S. S. (2024). Advances in Organic Materials for Next-Generation Optoelectronics: Potential and Challenges. *Organics*, *5*(4), Article 4. https://doi.org/10.3390/org5040028

Pramanik, M. B., Rakib, M. A. A., Siddik, M. A., & Bhuiyan, S. (2024). Doping Effects and Relationship between Energy Band Gaps, Impact of Ionization Coefficient and Light Absorption Coefficient in Semiconductors. *European Journal of Engineering and Technology Research*, *9*(1), Article 1. https://doi.org/10.24018/ejeng.2024.9.1.3118

Raship, N. A., Tawil, S. N. M., Nayan, N., & Ismail, K. (2023). Effect of Al Concentration on Structural, Optical and Electrical Properties of (Gd, Al) Co-Doped ZnO and Its n-ZnO/p-Si (1 0 0) Heterojunction Structures Prepared via Co-Sputtering Method. *Materials*, *16*(6). https://doi.org/10.3390/ma16062392

Rasmussen, F. A., & Thygesen, K. S. (2015). Computational 2D Materials Database: Electronic Structure of Transition-Metal Dichalcogenides and Oxides. *The Journal of Physical Chemistry C*, *119*(23), 13169–13183. https://doi.org/10.1021/acs.jpcc.5b02950

Rouzhahong, Y., Wushuer, M., Mamat, M., Wang, Q., & Wang, Q. (2020). First Principles Calculation for Photocatalytic Activity of GaAs Monolayer. *Scientific Reports*, *10*(1), Article 1. https://doi.org/10.1038/s41598-020-66575-9

Saadu Itas, Y., Razali, R., Khandaker, M. U., Tata, S., & Boukhris, I. (2024). Structural, mechanical, electronic and optical properties of Si decorated zinc oxide nanotube photocatalyst for hydrogen evolution via overall water splitting: A DFT study. *Physica B: Condensed Matter*, *673*, 415493. https://doi.org/10.1016/j.physb.2023.415493

Samaki, S., Tchangnwa Nya, F., Dzifack Kenfack, G. M., & Laref, A. (2023). Materials and interfaces properties optimization for high-efficient and more stable RbGeI3 perovskite solar cells: Optoelectrical modelling. *Scientific Reports*, *13*(1), Article 1. https://doi.org/10.1038/s41598-023-42471-w

Scarpa, D., Iuliano, M., Cirillo, C., Iovane, P., Borriello, C., Portofino, S., Ponticorvo, E., Galvagno, S., & Sarno, M. (2024). Self-assembled monolayers of reduced graphene oxide for robust 3D-printed supercapacitors. *Scientific Reports*, *14*, 14998. https://doi.org/10.1038/s41598-024-65635-8

Surnev, S., Goniakowski, J., Mohammadi, M., Noguera, C., & Netzer, F. P. (2024). Reduction of a two-dimensional crystalline MoO3 monolayer. *Surface Science*, *750*, 122579. https://doi.org/10.1016/j.susc.2024.122579

Tiwari, S. K., Sahoo, S., Wang, N., & Huczko, A. (2020). Graphene research and their outputs: Status and prospect. *Journal of Science: Advanced Materials and Devices*, *5*(1), 10–29. https://doi.org/10.1016/j.jsamd.2020.01.006

Wang, J., Mu, X., Sun, M., & Mu, T. (2019). Optoelectronic properties and applications of graphene-based hybrid nanomaterials and van der Waals heterostructures. *Applied Materials Today*, *16*, 1–20. https://doi.org/10.1016/j.apmt.2019.03.006

Wu, S., Senevirathna, H. L., Weerasinghe, P. V. T., & Wu, P. (2021). Engineering Electronic Structure and Band Alignment of 2D Mg(OH)2 via Anion Doping for Photocatalytic Applications. *Materials*, *14*(10), Article 10. https://doi.org/10.3390/ma14102640

Yang, J., Liu, K., Chen, X., & Shen, D. (2022). Recent advances in optoelectronic and microelectronic devices based on ultrawide-bandgap semiconductors. *Progress in Quantum Electronics*, *83*, 100397. https://doi.org/10.1016/j.pquantelec.2022.100397

Znidi, F., Morsy, M., & Nizam Uddin, Md. (2024). Recent advances of graphene-based materials in planar perovskite solar cells. *Next Nanotechnology*, *5*, 100061. https://doi.org/10.1016/j.nxnano.2024.100061

Zou, W., Lou, B., Kurboniyon, M. S., Buryi, M., Rahimi, F., Srivastava, A. M., Brik, M. G., Wang, J., & Ma, C. (2024). Unraveling Broadband Near-Infrared Luminescence in Cr3+-Doped Ca3Y2Ge3O12 Garnets: Insights from First-Principles Analysis. *Materials*, *17*(7), Article 7. https://doi.org/10.3390/ma17071709